

A Tale of Three Mysterious Spectral Features in Carbon-Rich Evolved Stars: The $21\ \mu\text{m}$, $30\ \mu\text{m}$, and “Unidentified Infrared” Emission Features

DRAFT: 2015.7.24.38

Ajay Mishra¹, Aigen Li¹, and B.W. Jiang²

ABSTRACT

The mysterious “ $21\ \mu\text{m}$ ” emission feature seen almost exclusively in the short-lived protoplanetary nebula (PPN) phase of stellar evolution remains unidentified since its discovery two decades ago. This feature is always accompanied by the equally mysterious, unidentified “ $30\ \mu\text{m}$ ” feature and the so-called “unidentified infrared” (UIR) features at 3.3 , 6.2 , 7.7 , 8.6 , and $11.3\ \mu\text{m}$ which are generally attributed to polycyclic aromatic hydrocarbon (PAH) molecules. The $30\ \mu\text{m}$ feature is commonly observed in all stages of stellar evolution from the asymptotic giant branch (AGB) through PPN to the planetary nebula phase. We explore the interrelations among the mysterious $21\ \mu\text{m}$, $30\ \mu\text{m}$, and UIR features of the $21\ \mu\text{m}$ sources. We derive the fluxes emitted in the observed UIR, $21\ \mu\text{m}$, and $30\ \mu\text{m}$ features from published *ISO* or *Spitzer*/IRS spectra. We find that none of these spectral features correlate with each other. This argues against a common carrier (e.g., thiourea) for both the $21\ \mu\text{m}$ feature and the $30\ \mu\text{m}$ feature. This also does not support large PAH clusters as a possible carrier for the $21\ \mu\text{m}$ feature.

Subject headings: circumstellar matter — dust, extinction — infrared: stars — stars: AGB and Post-AGB — stars: evolution

1. Introduction

In carbon-rich evolved objects, there are two prominent, mysterious emission bands known as the “ $21\ \mu\text{m}$ ” and “ $30\ \mu\text{m}$ ” spectral features (see Jiang et al. 2010). The enigmatic $21\ \mu\text{m}$ emission feature was first detected in four protoplanetary nebulae (PPNe) through the 7.7 – $22.6\ \mu\text{m}$ spectra obtained by the *Low Resolution Spectrometer* (LRS) on board the *Infrared Astronomical Satellite* (IRAS; Kwok et al. 1989). To date, this feature has been seen unambiguously in ~ 18 objects in the Milky Way (Cerrigone et al. 2011) and ~ 9 objects in the Large and Small Magellanic Clouds

¹Department of Physics and Astronomy, University of Missouri, Columbia, MO 65211, USA; amishra@mail.missouri.edu, lia@missouri.edu

²Department of Astronomy, Beijing Normal University, Beijing 100875, China; bjiang@bnu.edu.cn

(Volk et al. 2011).¹ The $21\ \mu\text{m}$ sources are all PPNe, objects in a rapid transition period (of several thousand years) between the asymptotic giant branch (AGB) and planetary nebula (PN) phases.² With a peak wavelength at $\sim 20.1\ \mu\text{m}$ and a FWHM of $\sim 2.2\text{--}2.3\ \mu\text{m}$, the $21\ \mu\text{m}$ feature displays little shape variation among different sources. This feature emits up to $\sim 8\%$ of the total infrared (IR) power of a $21\ \mu\text{m}$ source. The carrier of this feature remains unidentified, despite the fact that over a dozen carrier candidates have been proposed, including inorganic materials: TiC (von Helden et al. 2000, but see Li 2003), SiS_2 (Goebel 1993), SiC (Speck & Hofmeister 2004, but see Jiang et al. 2005), SiO_2 -coated SiC (Posch et al. 2004), carbon-silicon mixtures (Kimura et al. 2005), FeO (Posch et al. 2004, but see Li et al. 2013), Fe_2O_3 and Fe_3O_4 (Cox 1990, but see Zhang et al. 2009a), and organic materials: Ti-coordinated caged carbon (Kimura et al. 2005), urea or thiourea (Sourisseau et al. 1992), polycyclic aromatic hydrocarbon (PAH), and hydrogenated amorphous carbon (HAC) (Buss et al. 1993, Justtanont et al. 1996). It is considered as “*one of the most interesting unresolved mysteries in astrochemistry*” (Kwok et al. 2002).

The $30\ \mu\text{m}$ feature, first discovered by Forrest et al. (1981) in several carbon stars and in two PNe through the *Kuiper Airborne Observatory* spectrometry, is very broad and strong, extending from $\sim 24\ \mu\text{m}$ to $\sim 45\ \mu\text{m}$ and accounting for up to $\sim 30\%$ of the total IR luminosity of a $30\ \mu\text{m}$ source (Volk et al. 2002). Unlike the $21\ \mu\text{m}$ feature which displays little shape variation, the $30\ \mu\text{m}$ feature varies in its peak wavelength and width among different sources (e.g., see Hrivnak et al. 2000, Hony et al. 2002).

The carrier of the $30\ \mu\text{m}$ feature also remains unidentified. Magnesium sulfide (MgS) solids have long been proposed as a candidate carrier (Goebel & Moseley 1985; Nuth et al. 1985; Jiang et al. 1999; Szczerba et al. 1999; Hony et al. 2002, 2003; Lombaert et al. 2012). However, Zhang et al. (2009b) recently ruled out MgS as a valid carrier since it would require too much S to account for the observed large amount of power emitted from the $30\ \mu\text{m}$ feature (also see Messenger et al. 2013, Otsuka et al. 2014).³

While so far the $21\ \mu\text{m}$ feature appears to be restricted to PPNe, the $30\ \mu\text{m}$ feature is more ubiquitously seen in a large number of carbon-rich objects at various evolutionary stages, including AGB stars, post-AGB stars and PNe (see Jiang et al. 2010, Zhang & Jiang 2008). We note that *the $30\ \mu\text{m}$ feature is seen in all $21\ \mu\text{m}$ sources*, although not all $30\ \mu\text{m}$ sources emit at the $21\ \mu\text{m}$ feature. Furthermore, all $21\ \mu\text{m}$ sources display the so-called “unidentified IR” (UIR) features at 3.3, 6.2,

¹In the Magellanic Clouds the total number of $21\ \mu\text{m}$ sources would be 13 if the marginal detection in the other four sources is included (Volk et al. 2011).

²A few weak detections of the $21\ \mu\text{m}$ feature have also been reported for their precursors – highly evolved carbon stars (Volk et al. 2000) and their successors – PNe (Hony et al. 2001, Volk 2003). These detections are yet not very conclusive as the $21\ \mu\text{m}$ feature claimed for these sources is considerably weak.

³Lombaert et al. (2012) modeled the $30\ \mu\text{m}$ feature of the extreme carbon star LL Peg with MgS dust. They argued that if MgS is in thermal contact with amorphous carbon and SiC, the amount of MgS required to reproduce the strength of the $30\ \mu\text{m}$ feature agrees with the solar abundance of sulfur.

7.7, 8.6 and $11.3\,\mu\text{m}$ (Hrivnak et al. 2008) which are commonly attributed to PAH molecules (Léger & Puget 1984, Allamandola et al. 1985).

To gain insight into the nature of the carriers of the $21\,\mu\text{m}$ and $30\,\mu\text{m}$ features, we select ten well-studied Galactic $21\,\mu\text{m}$ sources. The $21\,\mu\text{m}$, $30\,\mu\text{m}$ and UIR features of these sources have been observationally obtained. This allows us to derive the fractional fluxes emitted respectively in the $21\,\mu\text{m}$, $30\,\mu\text{m}$ and UIR features (see §2). We examine in §3 the interrelations among the $21\,\mu\text{m}$, $30\,\mu\text{m}$ and UIR features in the selected $21\,\mu\text{m}$ sources. We discuss in §4 the implications of these interrelations. §5 discusses the methods of deriving the fluxes of the $21\,\mu\text{m}$, $30\,\mu\text{m}$ and UIR features. We summarize the major results in §6.

2. Deriving the Fluxes of the $21\,\mu\text{m}$, $30\,\mu\text{m}$ and UIR Features

We have selected ten well-studied Galactic $21\,\mu\text{m}$ sources. For these sources, the high-quality mid-IR spectra obtained by the *Spitzer Space Telescope* and the *Infrared Space Observatories* (ISO) allow one to measure relatively accurately the (integrated) fluxes emitted in the $21\,\mu\text{m}$ feature (F_{21}), in the $30\,\mu\text{m}$ feature (F_{30}), and in the UIR features (F_{UIR}).⁴ In Table 1 we tabulate the stellar and circumstellar parameters of the ten Galactic $21\,\mu\text{m}$ sources (compiled from the literature): the effective temperature T_{eff} , luminosity L_{\star} , core mass M_{\star} , stellar radius r_{\star} , and distance d from Earth of the central star.

Below we briefly comment on the individual sources, focusing on the nebular morphology of each source. *IRAS 02229+6208* is a cool, highly reddened post-AGB star. It has an elliptically extended nebula as revealed by the polarization map of Ueta et al. (2005). *IRAS 04296+3429* is in the advanced post-AGB evolution stage with a bipolar lobe structure as revealed by the scattered light images at 0.56 and $0.81\,\mu\text{m}$ (Sahai 1999). *IRAS 05341+0852* has a very extended, optically thin atmosphere. Its visible image shows an elongated elliptical nebula around the central star (Ueta et al. 2000). *IRAS 07134+1005* (*HD 56126*) is one of the best studied post-AGB star. It has an axial symmetric structure (Meixner et al. 1997; Ueta et al. 2000). It is one of the sources in which the $21\,\mu\text{m}$ and $30\,\mu\text{m}$ features were first discovered (Forrest et al. 1981, Kwok et al. 1989). *IRAS 16594-4656* is a bipolar post-AGB star as indicated by its dust emission spectral energy distribution (Meixner et al. 1999; Hrivnak et al. 2008). It has an optically thick circumstellar envelope. *IRAS 20000+3239* has an extended and axisymmetric bipolar structure as revealed by the near-IR imaging polarimetry of this object (Gledhill et al. 2001). For *IRAS 22223+4327*, the polarization map reveals an extended, optically thick circumstellar envelope (Gledhill et al. 2001). *IRAS 22272+5435* is extremely carbon-rich and fairly bright both in the IR and optical (Ueta et al. 2001). *IRAS 22574+6609* is very faint in the visible. It shows a bipolar morphology with a

⁴To have a full count of the $21\,\mu\text{m}$, $30\,\mu\text{m}$, and UIR fluxes, we require that the IR spectra of the selected sources at least cover the wavelength range of $\sim 5\text{--}35\,\mu\text{m}$. As a result of this criterion, the $21\,\mu\text{m}$ sources which lack the IR spectra at $\lambda < 10\,\mu\text{m}$ are not included in this study.

dark lane dividing the nebula into two lobes (Ueta et al. 2000; Su et al. 2001). *IRAS 23304+6147* has a quadrupolar shape, although its two pairs of lobes are not well separated. This object is remarkably similar to IRAS 20000+3239 in its post-AGB properties and AGB ejecta (Sahai et al. 2007).

We retrieve the IR spectra of the selected sources from the *Spitzer* and ISO archives. All sources exhibit the 21 μm , 30 μm and UIR features. In order to quantify the relative contributions from different components, we perform spectral decomposition of the IR spectra of these sources. Following Zhang et al. (2010), we use the IDL package PAHFIT of Smith et al. (2007) to decompose the observed IR spectra into individual components, including contributions from stellar continuum, H₂ lines, thermal dust continuum, and the 21 μm , 30 μm and UIR features. This decomposition technique will be discussed in §5. We note that the decomposition is not really a physical dust model. It only serves to measure the fluxes in the features.

The stellar continuum is assumed to be a blackbody of T_{eff} , the stellar effective temperature. In all cases, the stellar contribution to the IR spectra is negligible. Following Zhang et al. (2010), we include eight H₂ S(0)–S(7) rotational lines because they are seen in the observed spectra and need to be subtracted in order to accurately determine the fluxes of the dust spectral features. The profiles of the H₂ lines are assumed to be Gaussian. A modified blackbody $I_{\lambda} \sim \lambda^{-2} B_{\lambda}(T)$ is adopted to simulate the dust thermal continuum, where $B_{\lambda}(T)$ is the Planck function of temperature T at wavelength λ . For all the sources the best-fit requires two components with different temperatures to describe the dust thermal continuum: a warm dust component with $T_W \sim 130\text{--}190\text{ K}$, and a cold component with $T_C \sim 60\text{--}90\text{ K}$. The 21 μm , 30 μm and UIR features are fitted with a number of Drude profiles $I_{\lambda} = I_0 \gamma^2 / \{(\lambda/\lambda_0 - \lambda_0/\lambda)^2 + \gamma^2\}$, where λ_0 is the central wavelength, I_0 is the central intensity, and γ is the fractional FWHM of each feature. The broad 30 μm feature is fitted by two or three subfeatures at 26, 30 and 33 μm .⁵ For the UIR features, we include all the PAH bands listed in Table 1 of Draine & Li (2007). The Drude profile is expected for classical damped harmonic oscillators (see Li 2009). It closely resembles a Lorentzian profile. Compared with a Gaussian profile, both the Drude profile and the Lorentzian profile have more extended wings. The 21 μm , 30 μm and UIR features are better fitted with Drude profiles than Gaussian profiles, while the H₂ lines are better fitted with Gaussian profiles.

The optimal fitting to the observed spectra is achieved through the Levenberg-Marquardt least-square algorithm implemented in the IDL package. We are able to obtain reasonably good fits to the observed spectra using this technique. In Figures 1–3 we show the spectral decomposition fitting to the ten sources. The fluxes emitted by the 21 μm , 30 μm and UIR features are listed in Table 2.

⁵The ISO/SWS spectroscopy suggested that the 30 μm feature consists of two subfeatures: a narrow feature at 26 μm and a broad one at 33 μm (Hrivnak et al. 2000, Volk et al. 2002). However, the two distinct components in the 30 μm feature are less prominent in the *Spitzer* spectra (see Hrivnak et al. 2009). Like Zhang et al. (2010), we find it practical to use two or three Drude profiles peaking at 26, 30 and 30 μm to represent this feature as they provide better fits to the data.

Also listed in Table 2 is F_{IR} , the dust continuum IR flux integrated over the 5–45 μm wavelength range.⁶ The uncertainties of the feature strengths are estimated using the full covariance matrix of the least square parameters as described in Smith et al. (2007).

3. Interrelations among the 21 μm , 30 μm and UIR Features

Let $M_{21\mu\text{m}}$, $M_{30\mu\text{m}}$, and M_{UIR} respectively be the mass of the carrier of the 21 μm , 30 μm , and UIR features. Let $\kappa_{\text{abs}}^{21\mu\text{m}}$, $\kappa_{\text{abs}}^{30\mu\text{m}}$, and $\kappa_{\text{abs}}^{\text{UIR}}$ respectively be the ultraviolet/visible mass absorption coefficient of the carrier of the 21 μm , 30 μm , and UIR features. It is reasonable to assume that the total masses of the carriers of these unidentified features ($M_{21\mu\text{m}}$, $M_{30\mu\text{m}}$, and M_{UIR}) are proportional to the total mass of the bulk dust (M_{dust}) in the shell, although the proportional factor may differ from one to another. Let f_{21} , f_{30} , and f_{UIR} respectively be the ratio of the mass of the carrier of the 21 μm , 30 μm , and UIR features to the mass of the bulk dust in a 21 μm source. With $F_{\text{IR}} \propto (M_{\text{dust}} \times L_{\star})$ we have $F_{21} \propto (M_{21\mu\text{m}} \times \kappa_{\text{abs}}^{21\mu\text{m}} \times L_{\star}) \propto (f_{21} \times M_{\text{dust}} \times L_{\star}) \propto (f_{21} \times F_{\text{IR}})$. Similarly, we have $F_{30} \propto (f_{30} \times F_{\text{IR}})$ and $F_{\text{UIR}} \propto (f_{\text{UIR}} \times F_{\text{IR}})$. Therefore, even if f_{30} does not correlate with f_{21} or f_{UIR} , F_{30} could still correlate with F_{21} and F_{UIR} through F_{IR} . Therefore, for a physically reasonable correlation study of the 21 μm , 30 μm and UIR features, one need to normalize F_{21} , F_{30} and F_{UIR} by F_{IR} , in order to cancel out their common proportionality to F_{IR} .

We explore the interrelations among the 21 μm , 30 μm and UIR features. We normalize the fluxes emitted from these features (F_{21} , F_{30} , F_{UIR}) by F_{IR} , the total near- to mid-IR emission in the wavelength range of 5–45 μm . This is to see what fractions of the total near- to mid-IR luminosity are being carried by these features.

We show in Figure 4 the interrelations of the fractional fluxes of the 21 μm , 30 μm and UIR features. It is clear from Figure 4 that these features are not correlated. This differs from Cerrigone et al. (2011) who reported a positive correlation between F_{UIR} and F_{21} and suggested that the abundances of the carrier of the UIR bands and of the carrier of the 21 μm feature may be linked together, possibly because of a common formation process. We attribute the difference to the fact that Cerrigone et al. (2011) did not normalize F_{UIR} and F_{21} by F_{IR} . We argue that the correlation between F_{21} and F_{UIR} found by Cerrigone et al. (2011) may merely reflect the fact that both F_{21} and F_{UIR} correlate with F_{IR} (i.e., with $M_{21\mu\text{m}} \propto M_{\text{dust}}$, $M_{30\mu\text{m}} \propto M_{\text{dust}}$, and $M_{\text{UIR}} \propto M_{\text{dust}}$, even if f_{30} does not correlate with f_{21} or f_{UIR} , $M_{30\mu\text{m}}$ could still correlate with $M_{21\mu\text{m}}$ and M_{UIR}).

⁶For IRAS 04296+3429, IRAS 05341+0852, and IRAS 22223+4327, the IR spectra are not available at $\lambda > 35 \mu\text{m}$. We derive F_{IR} for these sources by extrapolating the observed spectra to $\lambda = 45 \mu\text{m}$.

Table 1: Stellar Parameters for the Ten Selected $21\ \mu\text{m}$ Sources.

IRAS Sources	T_{eff} (K)	L_{\star} (L_{\odot})	M_{\star} (M_{\odot})	r_{\star} (R_{\odot})	d (kpc)
02229+6208	5500	8333	0.558	98.4	2.1
04296+3429	6500	8333	0.554	69.1	5.0
05341+0852	6500	8430	0.551	69.5	7.8
07134+1005	7250	6554	0.841	49.0	2.2
16594-4656	10000	10279	0.60	32.0	2.55
20000+3239	5500	5186	...	77.0	2.24
22223+4327	6500	6075	0.551	59.0	3.2
22272+5435	5650	10990	0.574	106.0	1.55
22574+6609	5500	8061	0.60	96.0	7.6
23304+6147	6750	8347	0.66	64.0	3.25

Table 2: Integrated Fluxes Emitted in the UIR (F_{UIR}), $21\ \mu\text{m}$ (F_{21}), and $30\ \mu\text{m}$ (F_{30}) Features as well as the Total Near- to Mid-IR Emission (F_{IR}) in the $\sim 5\text{--}45\ \mu\text{m}$ Wavelength Range, as Derived from the PAHFIT Decomposition Method.

IRAS Sources	Warm Dust T_W (K)	Cold Dust T_C (K)	UIR ($10^{-12}\ \text{W m}^{-2}$)	F_{21} ($10^{-12}\ \text{W m}^{-2}$)	F_{30} ($10^{-12}\ \text{W m}^{-2}$)	F_{IR} ($10^{-12}\ \text{W m}^{-2}$)
02229+6208	160	90	5.78 ± 0.016	0.322 ± 0.002	9.10 ± 0.138	25.6 ± 1.95
04296+3429	185	61	0.870 ± 0.006	0.302 ± 0.002	1.62 ± 0.012	7.15 ± 0.23
05341+0852	190	70	0.283 ± 0.005	0.023 ± 0.008	0.35 ± 0.002	1.66 ± 0.07
07134+1005	160	90	1.84 ± 0.017	1.40 ± 0.002	2.88 ± 0.015	17.3 ± 1.60
16594-4656	135	78	3.25 ± 0.014	2.57 ± 0.002	9.97 ± 0.080	43.6 ± 2.90
20000+3239	158	80	0.522 ± 0.009	0.185 ± 0.001	2.63 ± 0.019	7.29 ± 1.50
22223+4327	150	70	0.158 ± 0.005	0.114 ± 0.001	0.986 ± 0.014	5.42 ± 0.30
22272+5435	165	90	4.22 ± 0.036	0.840 ± 0.010	11.4 ± 0.135	35.8 ± 2.20
22574+6609	170	60	0.734 ± 0.008	0.144 ± 0.002	1.20 ± 0.006	4.61 ± 0.69
23304+6147	165	89	0.767 ± 0.011	0.416 ± 0.001	2.88 ± 0.010	8.90 ± 0.83

Note. — For IRAS 04296+3429, IRAS 05341+0852, and IRAS 22223+4327, the IR spectra are not available at $\lambda > 35\ \mu\text{m}$. We derive F_{IR} for these sources by extrapolating the observed spectra to $\lambda = 45\ \mu\text{m}$.

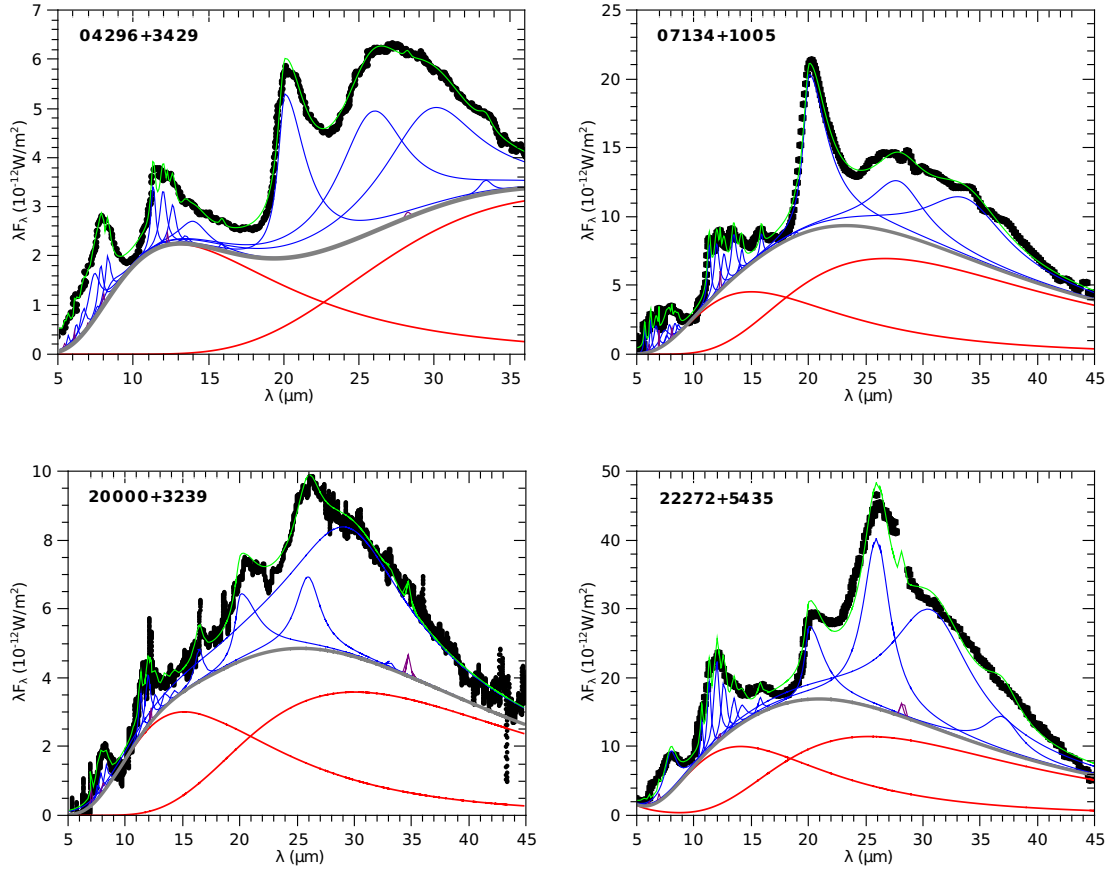


Fig. 1.— Decomposition of the observed IR spectra (black points) of the $21\,\mu\text{m}$ sources (IRAS 04296+3429, IRAS 07134+1005, IRAS 20000+3239, and IRAS 22272+5435) into a stellar continuum (pink line), two dust thermal continuum emission components (red lines), the $21\,\mu\text{m}$, $30\,\mu\text{m}$ and UIR features (blue lines), and the H_2 bands (violet lines). The decomposition is done with the PAHFIT technique. Gray lines are the sum of the stellar and dust thermal continuum. Green lines show the resulting model spectra.

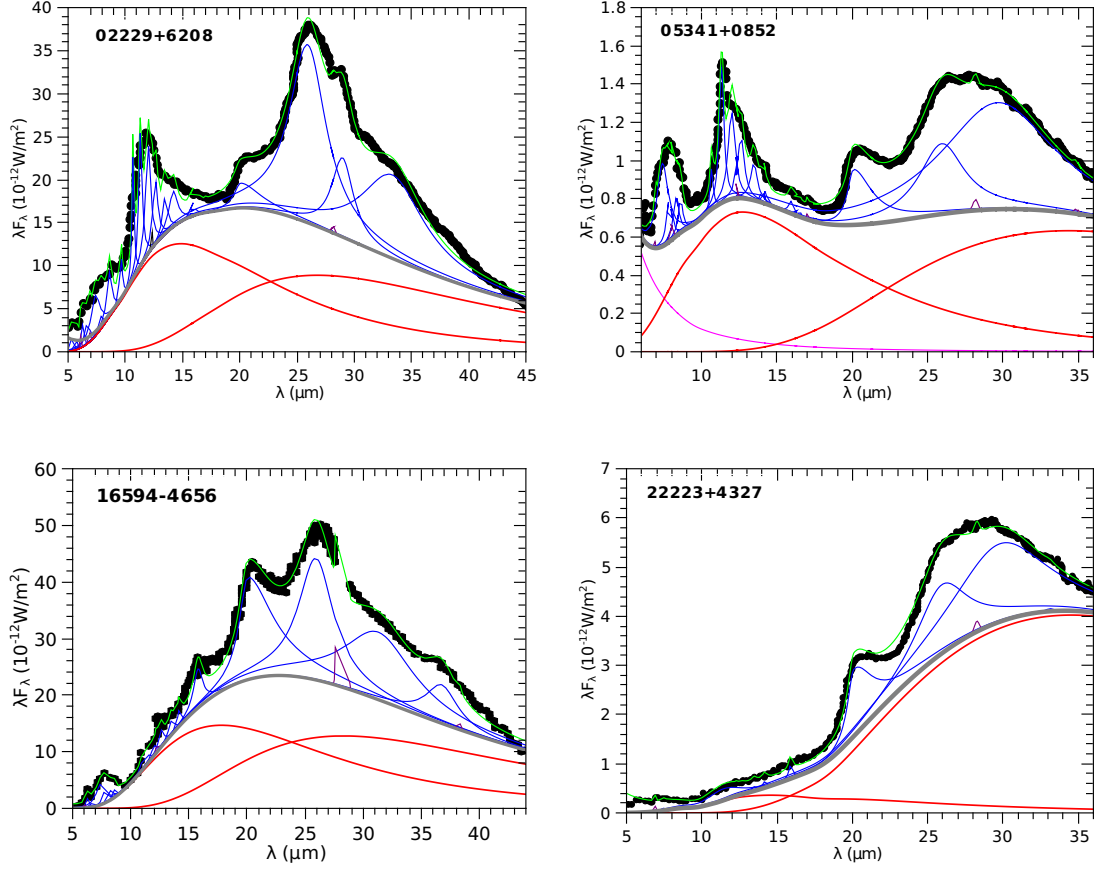


Fig. 2.— Same as Figure 1 but for IRAS 02229+6208, IRAS 05341+0852, IRAS 16594-4656, and IRAS 22223+4327.

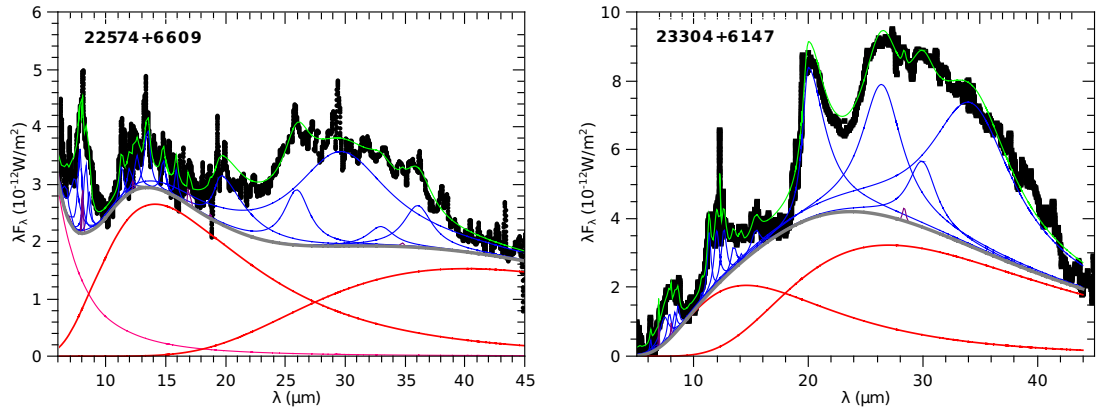


Fig. 3.— Same as Figure 1 but for IRAS 22574+6609 and IRAS 23304+6147.

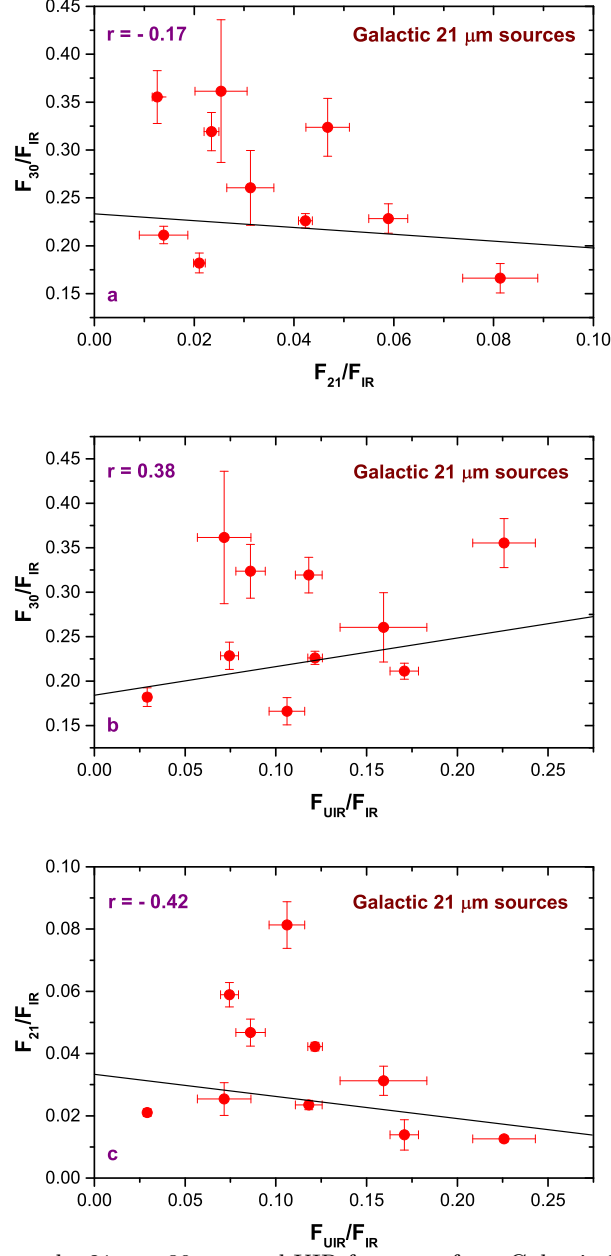


Fig. 4.— Interrelations among the 21 μm , 30 μm , and UIR features of ten Galactic 21 μm sources: (a) F_{30} vs. F_{21} , (b) F_{30} vs. F_{UIR} , and (c) F_{21} vs. F_{UIR} . All quantities are normalized by F_{IR} , the total near- to mid-IR emission obtained by *ISO* or *Spitzer* in the 5–45 μm wavelength range, to cancel out their common proportionality to F_{IR} . The fluxes emitted in the 21 μm , 30 μm , and UIR features are derived from the PAHFIT decomposition method.

4. Implications

The UIR bands are commonly attributed to PAH molecules. If the $21\,\mu\text{m}$ feature is due to large PAH clusters (Buss et al. 1990), F_{21} and F_{UIR} should be somewhat correlated: the fast stellar wind from the central star during the PPN phase might shatter PAH clusters into PAH molecules, possibly obliterating the carrier of the $21\,\mu\text{m}$ feature. The lack of correlation between F_{UIR} and F_{21} indicates that the $21\,\mu\text{m}$ feature is probably not due to large PAH clusters.

Papoular (2000, 2011) hypothesized that macromolecules with thiourea functional groups and aliphatic chains (made of CH_2 groups, oxygen bridges and OH groups) attached to various carbonaceous structures (mainly compact and linear aromatic clusters) are responsible for the $21\,\mu\text{m}$, $30\,\mu\text{m}$, and UIR features, with thiourea emitting the $21\,\mu\text{m}$ feature, the aliphatic chains producing the $30\,\mu\text{m}$ feature, and the aromatic clusters giving rise to the UIR bands. If this is the case, one would expect the $21\,\mu\text{m}$, $30\,\mu\text{m}$ and UIR features to be positively correlated. The lack of any positive correlation among these features as demonstrated in §2 does not support the hypothesis of Papoular (2000, 2011).

Volk et al. (2011) reported an anti-correlation between the $30\,\mu\text{m}$ and UIR features for the Magellanic Cloud $21\,\mu\text{m}$ sources. They postulated there may be some competition in forming the UIR and $30\,\mu\text{m}$ feature carriers. Indeed, if the $30\,\mu\text{m}$ feature is due to hydrogenated amorphous carbon (HAC), such an anti-correlation could result from radiation-induced decomposition of HAC grains into PAHs (Scott et al. 1997) and/or stellar wind-induced shattering of HAC grains into PAHs. However, as shown in Figure 4 for the Galactic $21\,\mu\text{m}$ sources the $30\,\mu\text{m}$ and UIR features do not seem to be anti-correlated.

Spectroscopically, the Magellanic Cloud $21\,\mu\text{m}$ sources differ appreciably from the Galactic $21\,\mu\text{m}$ sources (see Volk et al. 2011): (1) the average $21\,\mu\text{m}$ feature strength for the Magellanic Cloud objects is smaller than that observed in the Galaxy; (2) the $30\,\mu\text{m}$ feature of the Magellanic Cloud sources carries less of the total mid-IR emission than is normally the case for the Galactic $21\,\mu\text{m}$ sources; (3) the UIR features of the Magellanic Cloud $21\,\mu\text{m}$ sources are typically twice as strong as in the Galactic sources, with the peak of the UIR emission often being higher than that of the $30\,\mu\text{m}$ feature; and (4) the Magellanic Cloud objects have more structure in their UIR spectra and show more variation in the shapes and strengths of the 7.7 and $8.6\,\mu\text{m}$ features than is observed in the Galactic $21\,\mu\text{m}$ sources; more particularly, most of the Galactic $21\,\mu\text{m}$ sources have “unusual” UIR properties compared to the typical interstellar UIR bands (e.g., the Galactic $21\,\mu\text{m}$ sources have a broad $8\,\mu\text{m}$ feature rather than separately resolved $7.7/8.6\,\mu\text{m}$ UIR features) while the Magellanic Cloud $21\,\mu\text{m}$ sources show more “normal” looking UIR features (see Peeters et al. 2002). The remarkable difference in the spectral appearance of the UIR features between the Galactic and Magellanic Cloud $21\,\mu\text{m}$ sources would potentially hold important clues for understanding how the physical and chemical conditions affect the chemical structures of the carriers of these unidentified features.

An unique characteristic of the mysterious $21\,\mu\text{m}$ feature is that it is almost *exclusively* seen in

the short-lived PPN phase of stellar evolution and always accompanied by the equally mysterious $30\,\mu\text{m}$ feature and UIR bands, while the $30\,\mu\text{m}$ feature is commonly observed in all late stages of stellar evolution from the AGB through the PPNe to the PNe phase (the UIR features are seen in PPNe and PNe, but not in AGB stars). This implies that the carriers of the $21\,\mu\text{m}$ feature are likely formed during the so-called superwind phase (e.g., see von Helden et al. 2000), which is a phase of high mass-loss where AGB stars lose the remaining stellar envelope, terminating their life on the AGB (see Renzini 1981). They may also be easily destroyed by the highly energetic photons available in PNe. We also note that while the UIR features are commonly seen in PPNe, PNe, and the ISM, they are usually not seen in the mid-IR spectra of carbon-rich AGB stars.⁷

Finally, we also note that, in addition to the variable $30\,\mu\text{m}$ feature (in contrast to the invariable $21\,\mu\text{m}$ feature),⁸ the overall shape of the *Spitzer* spectra of the $21\,\mu\text{m}$ sources show also a lot of diversity, from having almost no flux at $\sim 10\,\mu\text{m}$ (like IRAS 22223-4327) to having a very flat spectrum (like IRAS 05341+0852, IRAS 22574+6609). We do not know what causes this diversity. We have examined the stellar luminosity, and the optical depth, the expansion history, and the inner and outer edges of the dust shell. They do not seem to be responsible for this overall spectral shape diversity.

5. PAHFIT Decomposition Versus Spline Fitting

When we use the PAHFIT decomposition method to derive the fluxes emitted from the $21\,\mu\text{m}$, $30\,\mu\text{m}$, and UIR features (see §2), we approximate the dust continuum with two modified blackbodies (see Figures 1,2). We admit that in dust spectral analysis the dust continuum determination is often notoriously difficult. This is true for studying PAHs (e.g., see Uchida et al. 2000), silicates (e.g., see Xie et al. 2014, Shao et al. 2014), and many other dust species. For the $21\,\mu\text{m}$ sources discussed in this work, what is the true dust continuum? Apparently, the fluxes of the dust spectral features are sensitive to the continuum determination. The key question here is to what extent the assumed continuum will affect the interrelations among these features examined in §3? To examine this, instead of approximating the dust continuum as two modified blackbodies, we take several points at $\sim 6\,\mu\text{m}$, $\sim 10\,\mu\text{m}$, $\sim 18\,\mu\text{m}$, $\sim 24\,\mu\text{m}$, and $\sim 44\,\mu\text{m}$ to define an underlying continuum and fit the continuum with a cubic spline function (see Figures 5,6). The $21\,\mu\text{m}$, $30\,\mu\text{m}$, and UIR fea-

⁷The few carbon stars that display the UIR features all have a hot companion that emits UV photons (Speck & Barlow 1997, Boersma et al. 2006). It has been argued that the carriers of the UIR features (e.g., PAHs) are present in carbon stars but are simply not excited sufficiently to emit at mid-IR due to lack of UV photons. However, Li & Draine (2002) have shown that the excitation of PAHs does not require UV photons, visible and near-IR photons are capable of exciting PAHs to emit at the UIR bands. The visible/near-IR cross sections measured by Mattiotta et al. (2005) for PAH ions imply that PAHs can be excited by the soft stellar photons from C stars. Therefore, the absence of the UIR bands in C stars places a limit on the abundance of small PAHs in these outflows.

⁸Hony et al. (2002) found that the peak wavelength of the $30\,\mu\text{m}$ feature shifts from $\sim 26\,\mu\text{m}$ in some AGB stars to $\sim 38\,\mu\text{m}$ in PN.

Table 3: Same as Table 2 but with the Dust Continuum Fitted with a Spline Function (See §5, and Figures 5,6).

IRAS Sources	UIR ($10^{-12} \text{ W m}^{-2}$)	F_{21} ($10^{-12} \text{ W m}^{-2}$)	F_{30} ($10^{-12} \text{ W m}^{-2}$)	F_{IR} ($10^{-12} \text{ W m}^{-2}$)
02229+6208	5.05 ± 0.57	0.34 ± 0.02	7.00 ± 0.58	25.6 ± 1.95
04296+3429	0.87 ± 0.06	0.35 ± 0.02	0.63 ± 0.06	7.15 ± 0.23
05341+0852	0.28 ± 0.04	0.029 ± 0.002	0.15 ± 0.01	1.66 ± 0.07
07134+1005	1.90 ± 0.30	1.62 ± 0.06	2.07 ± 0.25	17.3 ± 1.60
16594-4656	3.46 ± 0.41	2.02 ± 0.041	4.10 ± 0.07	43.6 ± 2.90
20000+3239	0.55 ± 0.09	0.19 ± 0.008	1.56 ± 0.11	7.29 ± 1.50
22223+4327	0.15 ± 0.02	0.10 ± 0.004	0.57 ± 0.05	5.42 ± 0.30
22273+5435	4.12 ± 0.61	0.89 ± 0.05	11.0 ± 0.71	35.8 ± 2.20
22574+6609	0.72 ± 0.10	0.11 ± 0.005	0.75 ± 0.12	4.61 ± 0.69
23304+6147	0.76 ± 0.09	0.54 ± 0.045	2.70 ± 0.36	8.90 ± 0.83

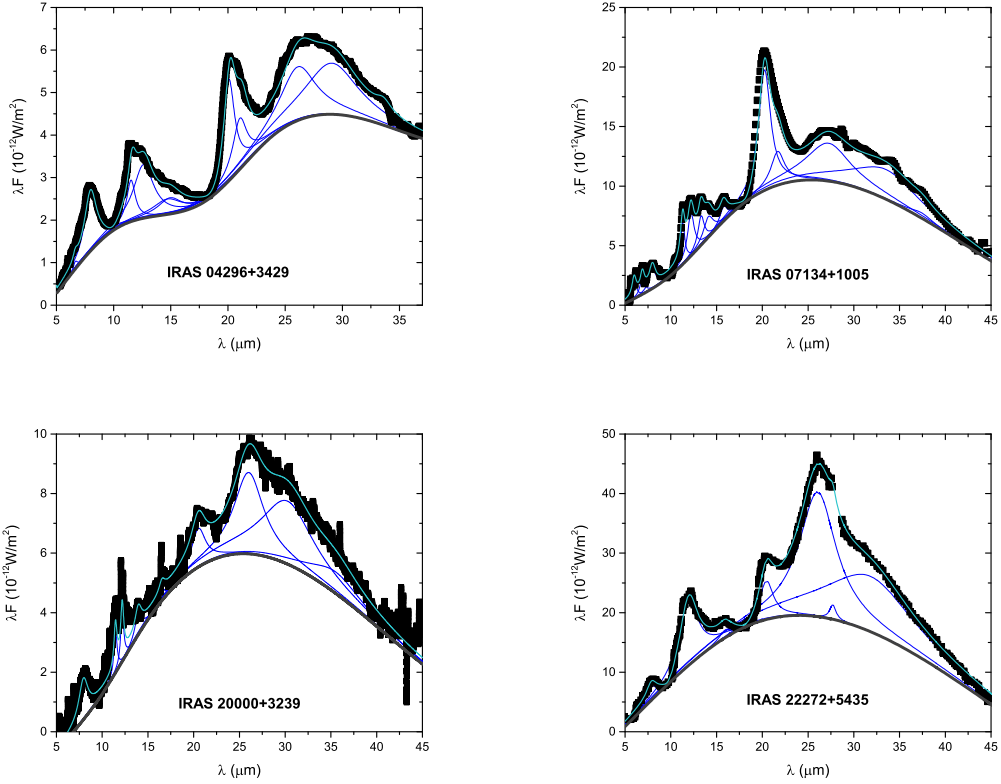


Fig. 5.— Same as Figure 1 but with the dust continuum fitted with a spline function instead of two modified blackbodies.

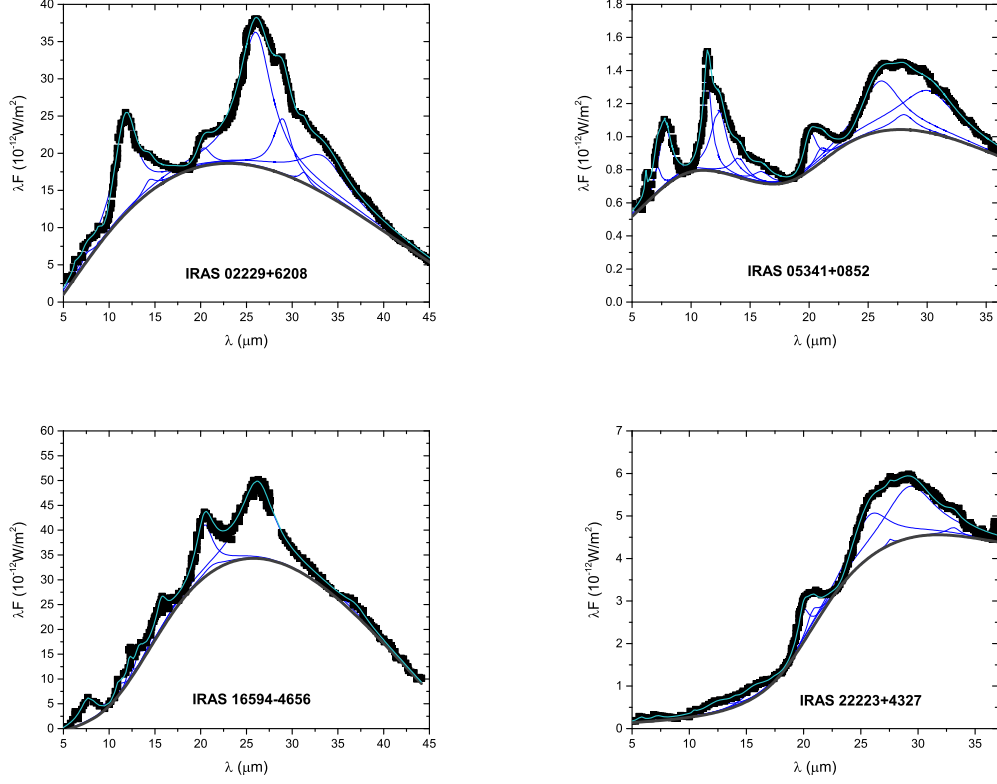


Fig. 6.— Same as Figure 2 but with the dust continuum fitted with a spline function instead of two modified blackbodies.

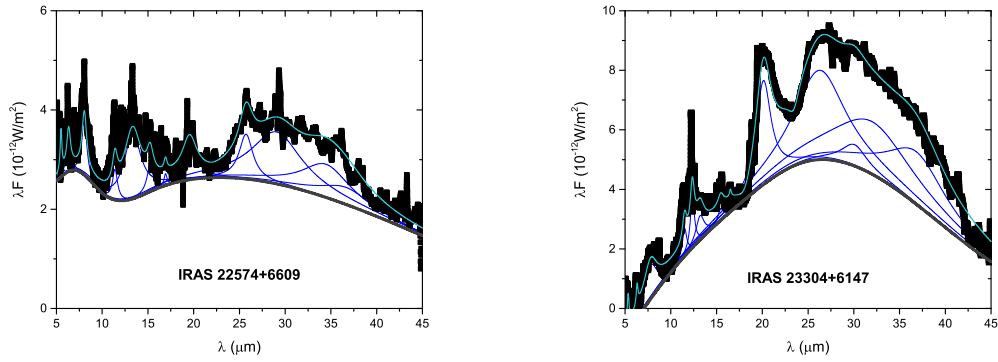


Fig. 7.— Same as Figure 3 but with the dust continuum fitted with a spline function instead of two modified blackbodies.

tures are again fitted with Drude profiles. In Table 3 we list the fluxes emitted in the $21\ \mu\text{m}$, $30\ \mu\text{m}$ and UIR features derived from the spline continuum method, as well as the dust IR flux integrated over the $5\text{--}45\ \mu\text{m}$ wavelength range. They differ from that of the PAHFIT decomposition method by $\sim 10\%$ for the $21\ \mu\text{m}$ and UIR features, and by $\sim 30\text{--}60\%$ for the $30\ \mu\text{m}$ feature. Figure 8 shows the interrelations of the fluxes of the $21\ \mu\text{m}$, $30\ \mu\text{m}$ and UIR features (normalized by the $5\text{--}45\ \mu\text{m}$ dust emission) derived from the spline continuum method. Similar to that obtained from the PAHFIT decomposition method, we see no correlation among these features. Therefore, we conclude that although the true dust continuum is not precisely known and the true fluxes emitted in the $21\ \mu\text{m}$, $30\ \mu\text{m}$ and UIR features are sensitive to the assumed continuum underneath the features, these features are unlikely correlated as demonstrated by the two very different continuum-determination methods.

6. Summary

We explore the interrelations among the mysterious $21\ \mu\text{m}$, $30\ \mu\text{m}$ and UIR features of the $21\ \mu\text{m}$ sources. The principal results are the following:

1. The $21\ \mu\text{m}$ feature does not correlate with the $30\ \mu\text{m}$ feature. This argues against the hypothesis of thiourea and aliphatic chains attached to various carbonaceous structures as the carriers for both the $21\ \mu\text{m}$ feature and the $30\ \mu\text{m}$ feature.
2. The $21\ \mu\text{m}$ feature does not correlate with the UIR features. This argues against large PAH clusters as a possible carrier for the $21\ \mu\text{m}$ feature.
3. The $30\ \mu\text{m}$ feature and the UIR features are not correlated. This does not support the speculation that the UIR carriers (e.g., PAHs) may result from the decomposition or shattering of the $30\ \mu\text{m}$ -feature carrier (e.g., HAC).

We thank Z. Ivezić, T. Ueta, K. Volk, Y.X. Xie, and K. Zhang for helpful discussions. We thank the anonymous referee for his/her very helpful suggestions which substantially improved the quality of this paper. We are supported in part by NSF AST-1109039, NNX13AE63G, NSFC 11173019, and the University of Missouri Research Board.

REFERENCES

- Allamandola, L.J., Tielens, A.G.G.M., & Barker, J.R. 1985, *ApJ*, 290, L25
- Bakker, J.E., van Dishoeck, E.F., Waters, L.B.F.M., & Schoenmaker, T. 1997, *A&A*, 323, 469
- Boersma, C., Hony, S., Tielens, A.G.G.M., 2006, *A&A*, 447, 213
- Buss, R. H., Jr., Cohen, M., Tielens, A. G. G. M., et al. 1990, *ApJ*, 365, L23

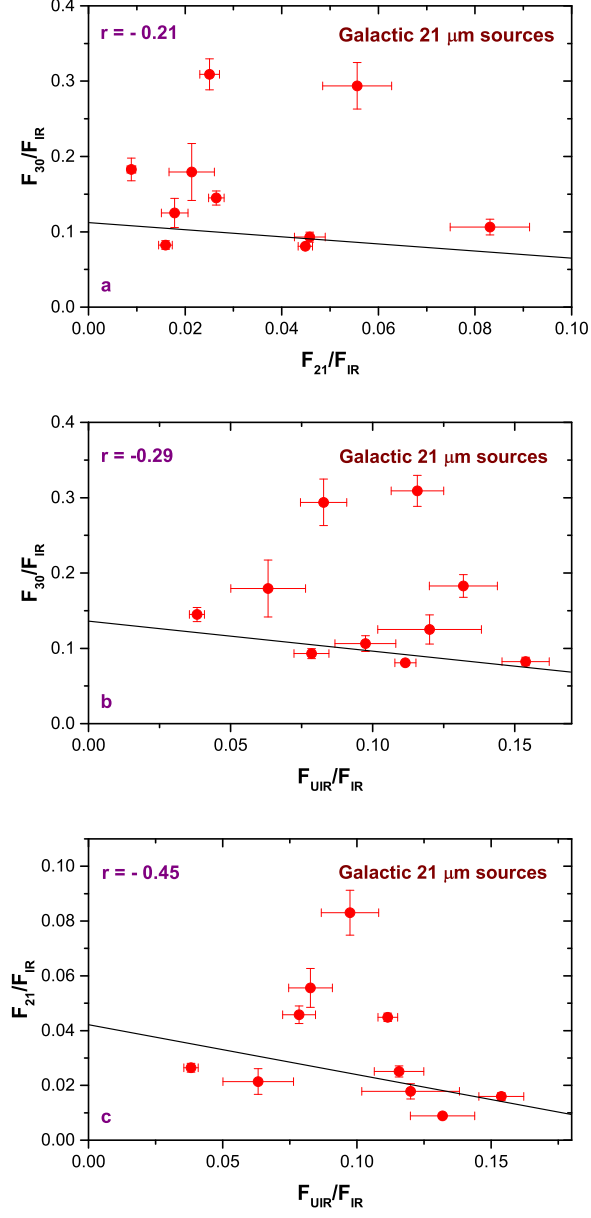


Fig. 8.— Same as Figure 4 but with the fluxes emitted in the 21 μm , 30 μm , and UIR features derived from the spline continuum method (see §5, and Figures 5,6).

- Cerrigone, L., Hora, J. L., Umana, G., Trigilio, C., Hart, A., & Fazio, G. 2011, *ApJ*, 738, 121
- Cox, P. 1990, *A&A*, 236, L29
- Draine, B.T., & Li, A. 2007, *ApJ*, 657, 810
- Forrest, W.J., Houck, J.R., & McCarthy, J.F. 1981, *ApJ*, 248, 195
- Gledhill, T.M., Chrysostomou, A., Hough, J.H., & Yates, J.A. 2001, *MNRAS*, 322, 321
- Goebel, J. H. 1993, *A&A*, 278, 226
- Goebel, J. H., & Moseley, S. H. 1985, *ApJ*, 290, L35
- Hony, S., Waters, L. B. F. M., & Tielens, A. G. G. M. 2001, *A&A*, 378, L41
- Hony, S., Waters, L. B. F. M., & Tielens, A. G. G. M. 2002, *A&A*, 390, 533
- Hony, S., Tielens, A. G. G. M., Waters, L. B. F. M., & de Koter, A. 2003, *A&A*, 402, 211
- Hony, S., & Bouwman, J. 2004, *A&A*, 413, 981
- Hrivnak, B. J., Volk, K., & Kwok, S. 2000, *ApJ*, 535, 275
- Hrivnak, B.J., & Biegging, J.H. 2005, *ApJ*, 624, 331
- Hrivnak, B.J., Volk, K., Geballe, T. R., & Kwok, S. 2008, in *Organic Matter in Space* (IAU Symp. 251), ed. S. Kwok & S.A. Sanford (Cambridge: Cambridge Univ. Press), 213
- Hrivnak, B. J., Volk, K., & Kwok, S. 2009, *ApJ*, 694, 1147
- Ivezić, Z., & Elitzur, M. 1997, *MNRAS*, 287, 799
- Jiang, B. W., Szczerba, R., & Deguchi, S. 1999, *A&A*, 344, 918
- Jiang B. W., Zhang K., Li A., 2005, *ApJ*, 630, L77
- Jiang, B. W., Zhang, K., & Li, A. 2010, *Earth, Planets, & Space*, 62, 105
- Justtanont, K., Skinner, C.J., Tielens, A.G.G.M., & Baas, F. 1996, *ApJ*, 456, 337
- Kimura, Y., Ishikawa, M., Kurumada, M., Tanigaki, T., Suzuki, H., & Kaito, C. 2005, *J. Cryst. Growth*, 275, 977
- Kimura, Y., Nuth, J.A. III, & Ferguson, F.T. 2005, *ApJ*, 632, L159
- Kwok, S., Volk, K., & Hrivnak, B. J. 1989, *ApJ*, 345, L51
- Kwok, S., Volk, K., & Hrivnak, B. J. 2002, *ApJ*, 573, 720

- Léger, A., & Puget, J.L. 1984, A&A, 137, L5
- Li, A. 2003, ApJ, 599, L45
- Li, A. 2009, Optical Properties of Dust, in Small Bodies in Planetary Sciences, ed. I. Mann, A. Nakamura, & T. Mukai, Springer, 167
- Li, A., & Draine, B.T. 2002, ApJ, 572, 232
- Li, A., Liu, J. M., & Jiang, B. W. 2013, ApJ, 777, 111
- Likkel, L., Forveille, T., Omont, A., & Morris, M. 1991, A&A, 246, 153
- Lombaert, R., de Vries, B.L., de Koter, A., Decin, L., Min, M., Smolders, K., Mutschke, H., & Waters, L.B.F.M. 2012, A&A, 544, L18
- Mattioda, A.L., Allamandola, L.J., & Hudgins, D.M. 2005, ApJ, 629, 1183
- Meixner, M., Skinner, C.J., Graham, J.R., Keto, E., Jernigan, J.G., & Arens, J.F. 1997, ApJ, 482, 897
- Meixner, M., Ueta, T., Dayal, A., Hora, J.L., Fazio, G., Hrivnak, B. J., Skinner, C. J., Hoffmann, W. F., & Deutsch, L. K. 1999, ApJs, 122, 221
- Messenger, S.J., Speck, A.K., & Volk, K. 2013, ApJ, 764, 142
- Nuth, J. A., Moseley, S. H., Silverberg, R. F., Goebel, J. H., & Moore, W. J. 1985, ApJ, 290, L41
- Omont, A., Loup, C., Forveille, T., Hekkert, P., Habing, H., & Sivagnanam, P. 1993, A&A, 267, 515
- Otsuka, M., Kemper, F., Cami, J., Peeters, E., & Bernard-Salas, J. 2014, MNRAS, 437, 2577
- Papoular, R. 2000, A&A, 362, L9
- Papoular, R. 2011, MNRAS, 415, 494
- Peeters, E., Hony, S., van Kerckhoven, C., et al. 2002, A&A, 390, 1089
- Posch, T., Mutschke, H., & Andersen, A.C. 2004, ApJ, 616, 1167
- Renzini, A. 1981, in Physical Processes in Red Giants, ed. I.A. Iben Jr. & A. Renzini (Dordrecht: Reidel), 431
- Sahai, R. 1999, ApJ, 524, L125
- Sahai, R., Morris, M., Contreras, C.S., & Claussen, M. 2007, ApJ, 134, 2200
- Scott, A., Duley, W. W., & Pinho, G. P. 1997, ApJ, 489, L193

- Smith, J.D.T., et al. 2007, *ApJ* , 656, 770
- Sourisseau, C., Coddens, G., & Papoular, R. 1992, *A&A*, 254, L1
- Speck, A.K., & Hofmeister, A.M. 2004, *ApJ*, 600, 986
- Speck, A.K., & Barlow, M.J. 1997, *Ap&SS*, 251, 115
- Su, K.Y.L., Hrivnak, B.J., & Kwok, S. 2001, *ApJ*, 122, 1525
- Szczerba, R., Henning, Th., Volk, K., Kwok, S., & Cox, P. 1999, *A&A*, 345, L39
- Uchida, K.I., Sellgren, K., Werner, M.W., & Houdashelt, M.L. 2000, *ApJ*, 530, 817
- Ueta, T., Meixner, M., & Bobrowsky, M. 2000, *ApJ*, 528, 861
- Ueta, T., Meixner, M., Hinz, P.M., et al. 2001, *A&A*, 557, 831
- Ueta, T., Murakawa, K., & Meixner, M. 2005, *AJ*, 129, 1625
- Volk, K. 2003, *Planetary Nebulae – Their Evolution and Role in the Universe (IAU Symp. 209)*, ed. S. Kwok, M. Dopita, & R. Sutherland (San Francisco, CA: ASP), 281
- Volk, K., Xiong, G.-Z., & Kwok, S. 2000, *ApJ*, 530, 408
- Volk, K., Kwok, S., Hrivnak, B. J., & Szczerba, R. 2002, *ApJ*, 567, 412
- Volk, K., Hrivnak, B.J., Matsuura, M., et al. 2011, *ApJ*, 735, 127
- von Helden, G., Tielens, A. G. G. M., van Heijnsbergen, D., et al. 2000, *Science*, 288, 313
- Xie, Y., Hao, L., & Li, A. 2014, *ApJ*, 794, L19
- Zhang, K., & Jiang, B.W. 2008, *Science in China: Physics, Mechanics and Astronomy*, 51, 1187
- Zhang, K., Jiang, B. W., & Li, A. 2009a, *MNRAS*, 396, 1247
- Zhang, K., Jiang, B. W., & Li, A. 2009b, *ApJ*, 702, 680
- Zhang, Y., Kwok, S., & Hrivnak, B. J. 2010, *ApJ*, 725, 990